**ROMANIAN JOURNAL OF INFORMATION SCIENCE AND TECHNOLOGY**
Volume **11**, Number 4, 2008, 409–422

# Plasma Surface Modification for Selective Hydrophobic Control

Marioara AVRAM[1], Andrei Marius AVRAM[1],
Adina BRAGARU[1], Andrei GHIU[1], Ciprian ILIESCU[2]

[1]National Institute for Research and Development in Microtechnologies,
Bucharest, P.O. Box 38-160, Romania

E-mail: marioara.avram@imt.ro

[2]Institute of Bioengineering and Nanotechnology, Singapore

E-mail: ciliescu@ibn.a-star.edu.sg

**Abstract.** The main objective of this research is theoretical and experimental investigation of the surfaces modification of $SU_8$, PDMS, $SiO_2$ and Si by RF plasma treatment. Physical-chemical reactions at room temperature can be used for the modifications of the surfaces in plasma, by modifying the contact angle, superficial polymerization, or by creating hydrophilic and/or hydrophobic regions on the surfaces in contact with plasma. The argon-plasma annealing was used for generate the hydrophilic surfaces, and plasma of $CF_4$ or $CF_4$ with $O_2$ has been used for creating of the hydrophobic surfaces.

## 1. Introduction

Microfluidic devices can be configured to imitate the functioning of semiconductor logical integrated circuits, such as switches, logical gates, flip-flop circuits and devices which can do Boolean and mathematical functions. Based on the observations that the interaction between two immiscible fluids can produce nonlinearities and instabilities inside microfluidic systems where the flow is laminar, and like any viscous flow through microchannels it can be characterized by a microfluidic resistance and capacity, simple microfluidic logical elements can be created. Theoretical explanations of their functioning can be found by further studying physical mechanisms that take place inside non-equilibrium dynamic systems: Rayleigh – Bernard convection, Taylor – Coutle flow inside solenoid systems [1]. The microfluidic resistor acts similar to the electric one. It forms during strong viscous flows between two terminals with a very

high pressure difference. Pressure differences will be created mainly by surface micromachining (plasma or chemical) by modifying the superficial tension. The microfluidic capacitor is represented by the high pressure reservoir and the unidirectional valve acts like a rectifier diode. For example, the simple circuit of a pump chamber with two control microvalves driven by pressure difference will be composed of two parallel microchannels, each with an associated microfluidic flow resistance and capacitance. If the pressure difference is positive one channel opens and if the pressure difference is negative, the other one opens. The microfluidic switch acts like a field effect transistor. The source-drain microchannel will be patterned into an elastomer deposited on a silicon or glass substrate and, in a second elastomer layer deposited on top of the first the gate the microchannel is microfabricated which will command fluid flow through the source-drain microchannel. In order to develop disposable microfluidic modules using passive valves as the flow-regulating components it is essential to work with a strongly hydrophobic substrate. In order to meet this goal it is necessary to use a naturally hydrophobic, low cost substrate. The polymer substrates are ideal choice for realization of microfluidic components. The polymer substrates are not necessarily the best solutions in all applications. For example in high temperature applications plastic substrates would be a highly inappropriate choice. Most engineering polymers: PMMA-poly-methyl-methacrylate, PC-poly-carbonate, PS–poly-styrene, PET-poly-ethylene-terephtelate and PDMS–poly-dimethyl-siloxane are hydro- phobic in nature, but the degree of hydrophobicity may not be enough for microfluidic applications. Hence, plasma surface modification techniques are explored to further increase the hydrophobicity of the polymer surfaces [1-2]. The main technological processes presented in this paper are: 1) selective functionalization / lithography – for optimizing / allowing detection functions. We will study the modifications of the photoresist, elastomer, glass surfaces after chemical and/or plasma treatments, and also the effects on the flow velocity and of the geometry on the performances in fluid transport through microchannels; 2) selective hydrophilic / hydrophobic lithography – in order to implement preprogrammed flow – variable geometries and selective covering of microchannels will be used to fabricate passive components (valves, filters, logical gates) and biological particle separation [3].

## 2. Theoretical Consideration

### 2.1. Structure of a RF plasma discharge

Plasma discharge consists of a large zone (the glow) with thin electrical boundary layers known as plasma sheaths. RF power is transferred to the electrons in the body of the plasma. When these electrons collide with neutral species in the plasma, molecules are fragmented, creating reactive free radicals. Some of the nascent free radicals are formed in excited states, other electron collision molecules without fragmenting them. Plasma volume is divided in three regions (Fig. 1). Ions go into the pre-sheath from the plasma volume with a flux density [4].

$$\Gamma_i = n_0\sqrt{\frac{kT_i}{2\pi m_i}}, \tag{1}$$

where $n_0$, $T_i$, and $m_i$ are ion quasineutral density, temperature and mass, and $k$ is Boltzmann constant. At the interface between the pre-sheath and sheath, the ion density is reduced by the Boltzmann exponential factor $n_i = n_0 \exp[-e(V - V_P)/kT_e]$ and the ion flux to the wafer surface is given by:

$$\Gamma_i = n_i\sqrt{\frac{kT_e}{2\pi m_i}}. \tag{2}$$

Electrons are rappelled in the sheath, so that ion and electron fluxes are equal at the wafer surface. The fraction of the volume electron flux that reaches wafer is given by the Boltzmann factor:

$$n_i\sqrt{\frac{kT_e}{2\pi m_i}} = n_0\sqrt{\frac{kT_i}{2\pi m_i}} \exp\frac{-\left(V_P - V_s\right)}{kT_e}. \tag{3}$$

The ion energy to the substrate is:

$$\varepsilon_i = e(V_P - V_s) \tag{4}$$

or

$$\varepsilon_i = \frac{\left(qE_0\right)^2}{8\pi^2\nu^2 m_i}, \tag{5}$$

where $q$ is ionic charge, $E_0$ is RF electric field, and $\nu$ is the RF frequency. Reactions like: e + molecule → atom + atom, can be characterized by the kinetic expression:

$$\frac{\mathrm{d}n_{atom}}{\mathrm{d}t} = n_e n_{mol} K(T_e, T_g), \tag{6}$$

where the rate constant $K(T_e, T_g)$ is the fraction of electron molecule collisions above the threshold energy for reaction, multiplied by the probability of the reaction.

$$K(T_e, T_g) = \int_0^\infty \sqrt{\frac{2\varepsilon}{m_e}}\sigma\left(\varepsilon\right) f\left(\varepsilon\right) \mathrm{d}\varepsilon, \tag{7}$$

where $\sigma(\varepsilon)$ is the cross section of the reaction and f$(\varepsilon)$ is the electron energy Boltzmann distribution [5].

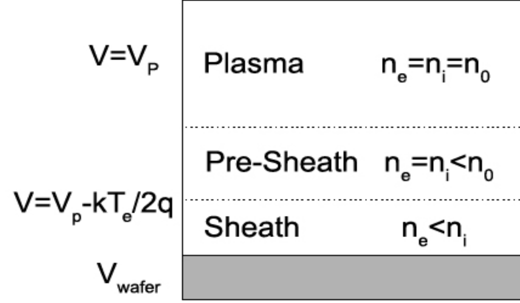


**Fig. 1.** Transition sheath and pre-sheath between plasma and wafer.

### 2.2. Plasma Physical Etching

The acceleration of the ions and electrons by the RF field is sinusoidal. Ions in general have a heavy mass, their motion is not in phase with RF field and their amplitude is small, but they have enough energy to cause sputtering. Energy given to the ions and electrons depends on the RF frequency, the distance between the electrodes and the RF power. Phenomena which can influence the behaviour of solids subjected to reactive ion bombardment are: diffusion of reactive species below the top surface of the substrate, physical sputtering, ion-induced damage (emphasising the effect of this damage on the chemical reactivity of the surface), and ions as a source of chemical reactants. The plasma particle and energy fluxes are calculated by solving a set of transport equations, which is valid for weakly collisional plasma. Boundary conditions are determined by solving global particle and energy balance equations, while the electric potential at the electrode is determined experimentally. Figure 2 shows the simulated dependence of the ion energy on the RF power. The ion energy is proportional to the voltage on the surface substrate (V), and the second one is proportional with square root of the RF power, as shown in Fig. 2. The physical etch rate due to the sputtering is given by [6]:

$$R_{phy} = \Gamma_i Y_i, \tag{8}$$

where $Y_i$ is the sputtering yield that is defined as the number of surface atoms ejected per incident ion, and $\Gamma_i$ is the perpendicular ions flux.

$$Y_i = \frac{20}{U_0} \left(Z_i Z_s\right)^2 \frac{m_i}{m_s} \left( \frac{\varepsilon}{\left(\varepsilon + 50 Z_i Z_s\right)^2} \right), \tag{9}$$

where $U_0$ is the surface binding energy (= 69.3 kcal/moll for SiC), $Z_i$, $Z_s$ the atomic numbers of ion and the substrate.

The simulated ion flux perpendicular to the electrode surface versus the RF power is plotted in Fig. 3. The etch rate for pure physical sputtering is directly proportional to the ion kinetic energy flux, in case of low pressure. Thus, the physical sputtering

profiles can be explained using the ion flux and energy profiles, which are given in Figs. 2 and 3.

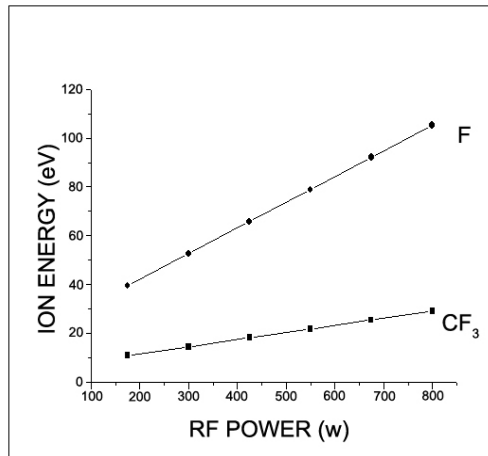


**Fig. 2.** Simulation results for ion ($F^-$ and $CF_3^+$) energy (eV) vs. RF power ($CF_4$ flowrate 40 sccm and 15% $O_2$).

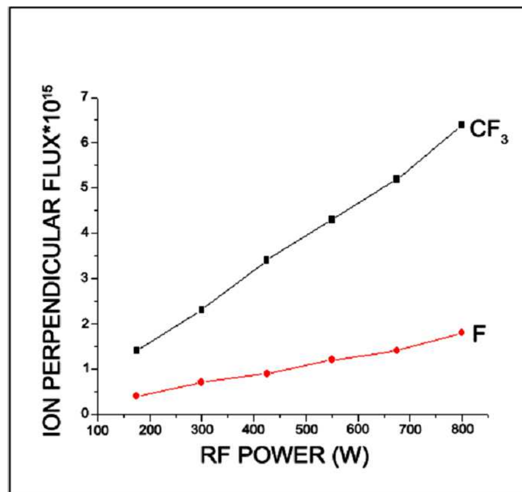


**Fig. 3.** Simulation results for ion ($F^-$ and $CF_3^+$) perpendicular flux ($10^{15}$ number of particles$\times$cm$^{-2}$) vs. RF power ($CF_4$ flowrate 40 sccm and 15% $O_2$).

### 2.3. Plasma Chemical Etching

The plasma is assumed to be a source of ionization that produces electrons and ions in according to the equations:

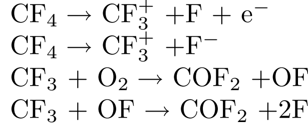

$CF_4 \rightarrow CF_3^+ + F + e^-$
$CF_4 \rightarrow CF_3^+ + F^-$
$CF_3 + O_2 \rightarrow COF_2 + OF$
$CF_3 + OF \rightarrow COF_2 + 2F$

Other ions are neglected because $CF_3^+$ is by far the predominant ion $CF_4$ and $CF_4/O_2$ discharges. The plasma-etching process can be viewed as serial sequence of steps, which are illustrated with SiC etching by fluorine.

1. Etchant formation;
2. Etchant transport to the surface;
3. Adsorption on the surface;
4. Etchant penetration through the product layer to virgin substrate;
5. Neutral and ion assisted products formation:
   $SiC + 4F + 2O \rightarrow SiF_4 + CO_2$,
   $2SiC + 4FO \rightarrow 2SiF_4 + 2CO_2$,
   $SiC + CF_4 + O_2 \rightarrow SiF_4 + 2CO$;
6. Neutral and ion-assisted products desorption.

The species for which the density is calculated in the model are $CF_4$, $CF_3$, $C_2F_6$ and F. The implemented reactions are given in Table 1 from the reference [5].

The electron continuity in the presence of ionization and attachment gives:

$$\frac{\partial n}{\partial t} + \nabla n_e v_e = n_e \left( v_i - v_a \right). \tag{10}$$

The ionisation and attachment are related on the electron distribution function $f_e$ by:

$$n_e v_{i,a} = \int N \sigma_{i,a} v f_e \mathrm{d}v. \tag{11}$$

Some authors assume an Arrenius form for chemical etching rate:

$$R_{chim} = Nk \exp(-E_a/kT_e). \tag{12}$$

In this paper is assumed that the Maxwell–Boltzmann distribution dominates the chemical etching rate that is a non-equilibrium state (eq.7), and can be tabulated as a function of mean energy by calculating the above integral numerically for different values of the electron temperature. The assumption of a Maxwell–Boltzmann distribution will generally be better at low pressure [8].

The total etch rate is a combination between physical and chemical etching rate [9].

$$R = \frac{B_1 \Gamma_{ion}^3 + B_2 \Gamma_{ion}^2 + B_3 \Gamma_{ion} \Gamma^2 + B_4 \Gamma^3}{A_1 \Gamma_{ion}^2 + A_2 \Gamma_{ion} \Gamma + A_3 \Gamma^2}, \tag{13}$$

where

$$\Gamma_{ion} = \sum_k \Gamma_k^{ion} \quad \text{and} \quad \Gamma = \sum_k \Gamma_k = \sum_k (\Gamma_k^{ion} + \Gamma_k^{neut}). \tag{14}$$

The $A_j$ and $B_j$ coefficients (j = 1, 2, 3, 4) are given by:

$$A_1 = Y_{ion}\left(\frac{U_0}{U_{poli}}\right)\left[Y_{ion}\left(\frac{U_0}{U_{dam}}\right) + Y_{d,cl}\right], \tag{15}$$

$$A_2 = Y_{d,cl}\varepsilon_{poli} + Y_{ion}\left(\frac{U_0}{U_{dam}}\right)\left[\varepsilon_{dam}\left(\frac{U_{dam}}{U_{poli}}\right) + \varepsilon_s + \varepsilon_{poli}\right], \tag{16}$$

$$A_3 = \varepsilon_{dam}\left(\varepsilon_s + \varepsilon_{poli}\right), \tag{17}$$

$$B_1 = Y_{ion}^2\left(\frac{U_0^2}{U_{poli}U_{dam}}\right)\left(Y_{ion} + Y_{d,cl}\right), \tag{18}$$

$$\begin{aligned} B_2 = Y_{ion}^2\left(\frac{U_0}{U_{dam}}\right)\left[\varepsilon_{dam}\left(\frac{U_{dam}}{U_{poli}}\right) + \varepsilon_{poli} + \varepsilon_s\left(\tfrac{U_0}{U_{poli}}\right) + \varepsilon_{cl}\left(\frac{U_0}{U_{poli}}\right)\right] + \\ + Y_{d,cl}Y_{ion}\left(\frac{U_0}{U_{poli}}\right)\left[\varepsilon_{dam} + \varepsilon_{poli}\left(\frac{U_{poli}}{U_{dam}}\right)\right], \end{aligned} \tag{19}$$

$$\begin{aligned} B_3 = \varepsilon_{dam}Y_{ion}\left[\varepsilon_{poli} + \varepsilon_s\left(\frac{U_0}{U_{poli}}\right)\right] + Y_{d,cl}\varepsilon_{dam}\varepsilon_{poli} + \\ + \varepsilon_{cl}Y_{ion}\left(\frac{U_0}{U_{dam}}\right)\left[\varepsilon_{dam}\left(\frac{U_{dam}}{U_{poli}}\right) + \varepsilon_{poli}\right] + \varepsilon_{poli}\varepsilon_s Y_{ion}\left(\frac{U_0}{U_{dam}}\right), \end{aligned} \tag{20}$$

$$B_4 = \varepsilon_{dam}\varepsilon_{poli}\left(\varepsilon_{cl} + \varepsilon_s\right), \tag{21}$$

$$C_1 = Y_{ion}^2\left(\frac{U_0^2}{U_{poli}U_{dam}}\right), \tag{22}$$

$$C_2 = Y_{ion}\left(\frac{U_0}{U_{dam}}\right)\left[\varepsilon_{dam}\left(\frac{U_{dam}}{U_{poli}}\right) + \varepsilon_{poli}\right], \tag{23}$$

$$C_3 = \varepsilon_{dam}\varepsilon_{poli}, \tag{24}$$

$$D_1 = Y_{ion}\left(\frac{U_0}{U_{poli}}\right)Y_{d,cl}, \tag{25}$$

$$D_2 = Y_{d,cl}\varepsilon_{poli}, \tag{26}$$

$$D_3 = 0, \tag{27}$$

$$F_1 = 0, \tag{28}$$

$$F_2 = Y_{ion} \left( \frac{U_0}{U_{dam}} \right) \varepsilon_s, \tag{29}$$

$$F_3 = \varepsilon_{dam} \varepsilon_s, \tag{30}$$

where:

$$Y_{ion} = \frac{\sum_k \Gamma_k^{ion} Y_k^{ion}}{\sum_k \Gamma_k^{ion}}, \quad Y_{d,cl} \frac{\sum_k \Gamma_k^{ion} Y_k^{d,cl}}{\sum_k \Gamma_k^{ion}},$$

$$\varepsilon_{cl} = \frac{\sum_k \Gamma_k \varepsilon_k^{cl}}{\sum_k \Gamma_k}, \quad \varepsilon_{dam} = \frac{\sum_k \Gamma_k \varepsilon_k^{dam}}{\sum_k \Gamma_k},$$

$$\varepsilon_{poli} = \frac{\sum_k \Gamma_k \varepsilon_k^{poli}}{\sum_k \Gamma_k}, \quad \varepsilon_s = \frac{\sum_k \Gamma_k \varepsilon_k^{s}}{\sum_k \Gamma_k},$$

$$f_{cl}^* = \frac{C_1 \Gamma_{ion}^2 + C_2 \Gamma_{ion} \Gamma_{neut} + C_3 \Gamma_{neut}^2}{A_1 \Gamma_{ion}^2 + A_2 \Gamma_{ion} \Gamma_{neut} + A_3 \Gamma_{neut}^2},$$

$$f_{dam}^* = \frac{D_1 \Gamma_{ion}^2 + D_2 \Gamma_{ion} \Gamma_{neut} + D_3 \Gamma_{neut}^2}{A_1 \Gamma_{ion}^2 + A_2 \Gamma_{ion} \Gamma_{neut} + A_3 \Gamma_{neut}^2},$$

$$f_{poli}^* = \frac{F_1 \Gamma_{ion}^2 + F_2 \Gamma_{ion} \Gamma_{neut} + F_3 \Gamma_{neut}^2}{A_1 \Gamma_{ion}^2 + A_2 \Gamma_{ion} \Gamma_{neut} + A_3 \Gamma_{neut}^2}.$$

$\varepsilon_k^{cl}$, $\varepsilon_k^{dam}$ and $\varepsilon_k^{poli}$ represents the probability that a particle which collides with the substrate to create a chemical reaction with atoms on the substrate. The binding energies of the substrate surface are denoted with $U_0$, $U_{dam}$ and respectively $U_{poli}$ for cleaning, damaging or polimerizing.

## 3. Effect of Plasma on Polymer Surfaces

Bio-microelectromechanical systems (BioMEMS) and microfluidic devices are usually built up from chemically inert materials such as silicon, glass, PDMS, PMMA, PC, PS, PET or SU-8 [10]. For microfluidic systems used in nano-bio applications, it is decisive to use fluids in the devices. Unfortunately, the most native surfaces are highly hydrophobic and they have low surface energy. This implies that microfluidic systems require active pumping mechanism. The polymer surfaces have to be rendered hydrophilic to enhance the capillary flow. Aim of this research is to develop

surface modification techniques, characterization of surface modification, and detailed analysis of the surface chemistry after plasma modification using experimental methods.

The reasons for choosing plasma treatment are:

(a) Facilities for plasma processing are available at IMT - Bucharest and the technique is familiar for most MEMS engineers.

(b) It is a relatively easy and fast process that can accomplish reliable surface modification.

(c) It is a parallel process suitable for high-volume, low-cost fabrication.

We propose the use of plasma surface treatment in a fluorinated environment that should increase the hydrophobicity of the surface. An empirical investigation of the various parameters that affect the results of the plasma treatment such as gas composition, duration of plasma, effect of RF power etc. was conducted to optimize the surface modification process. The simplest plasma configuration is that of parallel-plate capacitive coupled plasma. The process gas is introduced into the plasma chambers at moderately low pressures (10–100 Pa). When RF energy is supplied to the electrode pair of the plasma chamber, it accelerates stray electrons, increasing their energy to the limit where they can break chemical bonds in the process gas and generate additional ions and electrons. This process multiplies as more and ions/electrons are generated until a stable discharge is achieved. The plasma chamber now consists of the discharge region (or glow region) and the sheath region (or dark region). The glow region of the plasma is almost neutral with equal number of electron/ions being generated and recombined. The low mass electrons can escape the glow region more easily and hence a self-bias is created in the sheath region. This bias inhibits motion of more electrons out of the bulk region and steady state plasma is achieved.

When a polymer is exposed to plasma the following effects can occur:

1) Etching reaction: The etching process can be further sub-divided into two steps namely surface cleaning (removal of organic contaminants) and ablation or etching of the material near the surface of the polymer. Typically low energy oxygen plasma is used for organic contaminant removal. When polymers are exposed to sufficiently high plasma power the top layer on the polymer is ablated. Chain-scission of the macromolecules is believed to be the main reason for this ablation process. Ablation can also alter the surface topography of the polymers exposed to plasma for a short duration improves their wettability without modifying their surface texture, but over-treatment gives a very porous surface.

2) Cross-linking or branching of near-surface molecules/ Free radical generation: the first part of this process is described by cross-linking via activated species of inert gases. When a polymer is exposed to inert gas plasmas (Ar), the energetic ion bombardment and the vacuum ultraviolet photons, $\lambda < 175$ nm, will break the C-C and C-H bonds. However, due to the inert gas composition, no new chemical functionalities are added to the surface. The free radicals generated

by this process will partially react with other free radicals or any impurities in the plasma gas (active species), which leads to cross-linking or branching of polymer chains near the surface. It is widely held that these radicals are fairly stable (even after the plasma is stopped and the sample is removed from the plasma chamber) and can react with ambient oxygen. The post-plasma radical reaction is believed to be the reason why oxygen functionalities such as carboxyl, hydroxyl etc. which can be observed on surfaces treated with inert gas plasmas.

3) Implantation reactions: this mechanism is the primary reason for using plasma surface modification. In plasma, (depending on the composition gases) oxygen, nitrogen, fluorine atoms exists in activated states that can easily react with the polymer surface. The degree of surface modification is dependent on the polymer material structure also. Most of the research is concentrated on using plasma surface modification to render plastic surfaces more hydrophilic for improved adhesion properties. In some special cases, fluorination of the surfaces is also desirable to improve the chemical resistance of the surface, providing anti-stiction coatings. It must be emphasized that there is no clear distinction between the three processes. Usually, all three processes are occurring simultaneously to varying degrees depending on the power, gas composition, duration and the polymer substrate itself.

## 4. Experimental Results

It was investigated the effect of various parameters of plasma (RF power, electrode potential, flow capacity of gases, plasma composition, pressure in reactor, time of exposure) about the contact angle of water on surfaces mentioned on the top, about the morphology of surfaces. We observed that $CF_4$ and $CF_4/O_2$ plasma was used to create hydrophobic surfaces and Argon plasma was used to generate hydrophilic surfaces.

For hydrophobic surface annealing, the $CF_4$ gas flow rate has very little effect on the contact angle as shown in Fig. 4. It is observed that the contact angle varies from $105° - 107°$ which is within the deviation range for multiple samples; hence it is reasonable to assume that $CF_4$ gas flow rate has little to no effect on the surface modification process. Surprisingly, a mixture of $O_2$ and $CF_4$ plasma can produce more hydrophobic surfaces. As shown in Fig. 6, increasing the oxygen flow rate from 0–80 sccm (for a fixed $CF_4$ flow rate of 30 sccm), increases the contact angle from $104° - 136°$. In fact, the highest possible contact angles are achieved when using a mixed of $O_2/CF_4$ ($O_2$ (20 sccm) + $CF_4$ (30 sccm)) rather than $CF_4$ alone. Using $O_2$ plasma, it is very difficult to control the contact angle in the hydrophilic zone. 2 minutes plasma annealing at RF power 50 W with oxygen, the contact angle drops dramatically to 90°. Hence, hydrophilic annealing was effected using Argon gas in plasma chamber.

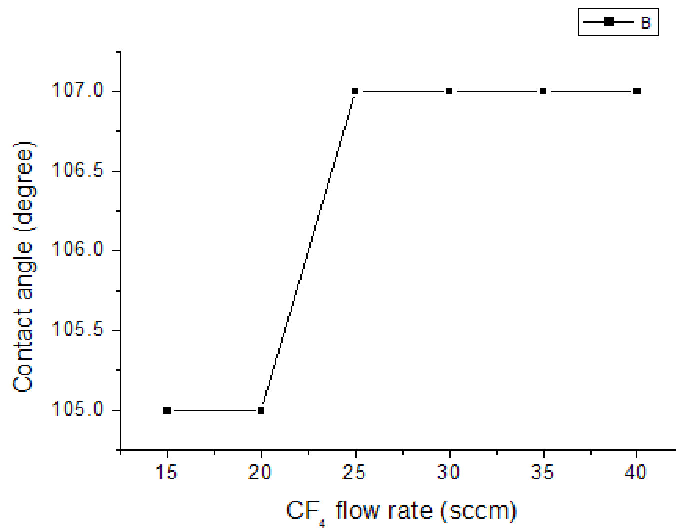


**Fig. 4.** Contact angle variation function of $CF_4$ flow rate. Power 50 W, Pressure 20 Pa, 2 min.

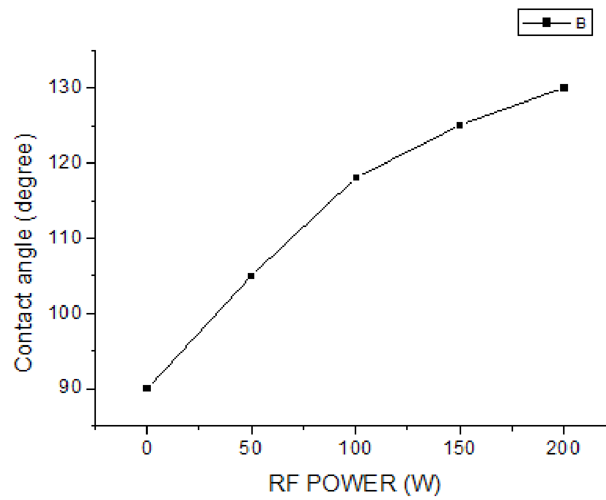


**Fig. 5.** Contact angle variation function of RF Power. $CF_4$ flow rate 20 sccm, Pressure 20 Pa, annealing time 4 min.

As mentioned previously, it is very difficult to control the contact angle using oxygen plasma for hydrophilic surface modification. With increasing power for Argon plasma a monotonic decrease in contact angle is observed as shown in Fig. 8. We

observed that the contact angle increase linearly by the decreasing of pressure in reactor and by increasing of RF power.

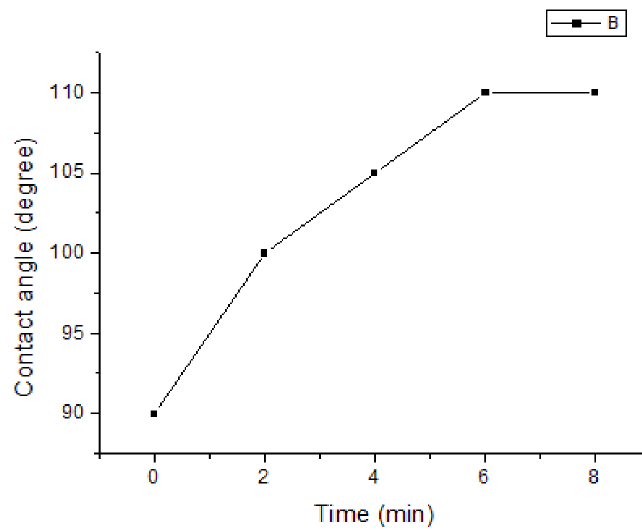


**Fig. 6.** Contact angle variation function of annealing time. $CF_4$ flow rate 30 sccm, Pressure 20 Pa, RF Power 50 W.

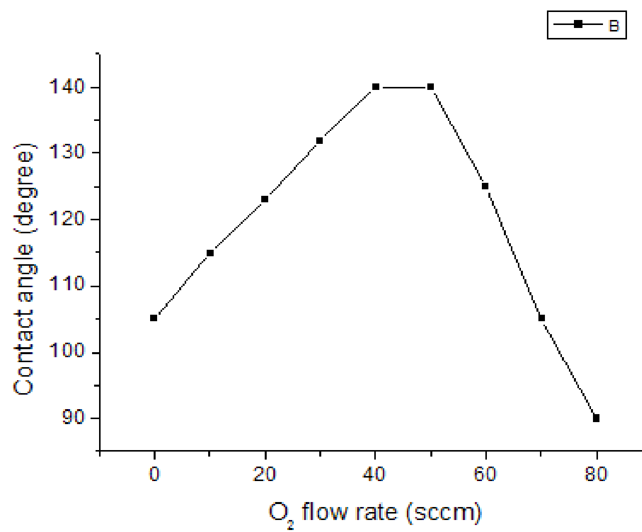


**Fig. 7.** Contact angle variation function of oxygen flow rate. $CF_4$ flow rate 20 sccm, Pressure 20 Pa, RF Power 50 W, annealing time 2 min.

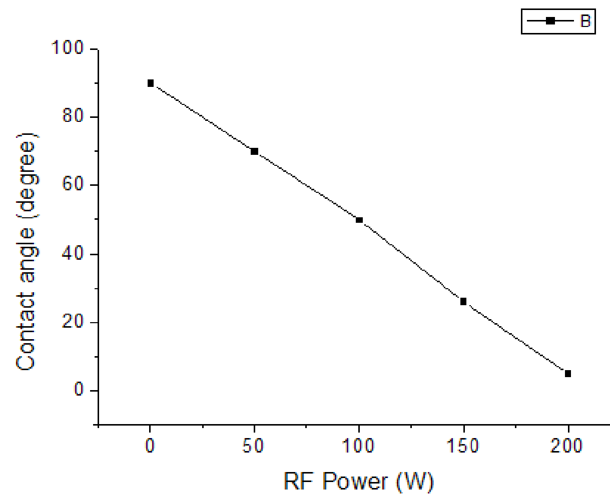


**Fig. 8.** Contact angle variation function of RF Power.
Ar flow rate 200 sccm, Pressure 20 Pa, annealing time 2 min.

## 5. Conclusions

A model of reactive ion etching has been presented. The model incorporates the gas phase reaction, the non-linear effects of physical effects and enhanced chemical etching. Physicals sputtering due to the formation of chemical compounds on the substrate surface with lower lattice displacement energy than the original substrate material. The increasing of chemical reactivity is a result of the changes in the chemical properties of the substrate surface due to the bombardment of the substrate. The etch rate found to have a non-linear dependence on ion particle flux and ion energy flux. It was investigated the effect of various parameters of plasma (RF power, electrode potential, flow capacity of gases, plasma composition, pressure in reactor, time of exposure) about the contact angle of water on surfaces mentioned on the top, about the morphology of surfaces. It has observed in fact that $O_2$ plasma drastically decreasing the contact angle, under 20°, and the $CF_4$ based plasmas determine a considerable increasing of contact angle, much than 110°. It has observed that the contact angle increasing from 105° to 135° by the increasing of $O_2$ flow capacity added to $CF_4$ plasma, from 0 to 100 sccm. It has observed that the contact vary little, from 105° to 110° on the increasing of $CF_4$ flow capacity. The contact angle drastically increases by the decreasing of pressure in reactor and by increasing of RF power.

# References

[1] GILBRECH D. A., *Fluid Mechanics*, pp. 270–275, 2001.

[2] WALTHER F., DAVIDOVSKAYA P., ZUCHER ST., KAISER M., HERBERG H., GIGLER A., STARK R., *Stability of the hydrophilic behaviour of oxygen plasma activated SU-8*, J. Micromech. Microeng, **17**, pp. 524–531, 2007.

[3] HO-JO B., VAN LERBERGHE L., MOTSEGOOD K., BEEBE D., *3D microchannel fabrication in PDMS elastomer*, J. MEMS, vol. **9**, no. 1, p. 76, 2000.

[4] CHAPMAN B., *Glow Discharge Process Sputtering and Plasma Etching*, Wiley, New York, 1980.

[5] EDELSON D., FLAMM D. L., J. Appl. Phys., **56**, p. 1522, 1984.

[6] YIH P. H., STECKL A. J., J. Electrochem. Soc., vol. **140**, 6, p. 1813, 1993.

[7] ZAWAIDEH E., KIM N. S., J. Appl. Phys., **64**, p. 4199, 1988.

[8] KIREEV P. S., *Semiconductor Physics*, 1974.

[9] AVRAM M., *A Silicon Carbide Reactive Ion Etching Model*, *Proc. of International Semiconductor Conference*, Oct. 7–11, Vol. **2**, pp. 523–526, 1998.

[10] LEE Y. Y., YU L., TAY F. E. H., ILIESCU C., *Characterisation of Spray Coating Photoresist for MEMS Applications*, ROMJIST, Vol. **8**, no. 4, pp. 383–390, 2005.